Dynamic structure factor of density fluctuations from direct imaging very near (both above and below) the critical point of SF_6

Ana Oprisan, Sorinel A. Oprisan, and Brittany Bayley
Department of Physics and Astronomy, College of Charleston, 66 George Street, Charleston, South Carolina 29424, USA

John J. Hegseth
Department of Physics, University of New Orleans, 2000 Lakeshore Drive, New Orleans, Louisiana 70148, USA

Yves Garrabos and Carole Lecoutre-Chabot
Institut de Chimie de la Matiere Condensee de Bordeaux, University de Bordeax I, Avenue de Dr. Schweitzer, F-33608 Pessac Cedex, France

Daniel Beysens
Institut de Chimie de la Matiere Condensee de Bordeaux, University de Bordeax I, Avenue de Dr. Schweitzer, F-33608 Pessac Cedex, France,
Equipe du Supercritique pour l'Environnement, les Matériaux et l'Espace, Physique et Mécanique des Milieux Hétérogènes, UMR 7636 CNRS-ESPCI - Université Paris 6 - Université Paris 7, 10 rue Vauquelin, 75231 Paris, France, and
Service des Basses Températures, Commissariat à l'Energie Atomique-Grenoble, 17, rue des Martyrs, 38504 Grenoble, France
(Received 12 August 2012; revised manuscript received 2 October 2012; published 3 December 2012)

Large density fluctuations were observed by illuminating a cylindrical cell filled with sulfur hexafluoride (SF_6), very near its liquid-gas critical point ($|T - T_c| < 300\ \mu$K) and recorded using a microscope with 3 μm spatial resolution. Using a dynamic structure factor algorithm, we determined from the recorded images the structure factor (SF), which measures the spatial distribution of fluctuations at different moments, and the correlation time of fluctuations. This method authorizes local measurements in contrast to the classical scattering techniques that average fluctuations over the illuminating beam. We found that during the very early stages of phase separation the SF scales with the wave vector q according to the Lorentzian q^{-2}, which shows that the liquid and vapor domains are just emerging. The critical wave number, which is related to the characteristic length of fluctuations, steadily decreases over time, supporting a sustained increase in the spatial scale of the fluctuating domains. The scaled evolution of the critical wave number obeys the universal evolution for the interconnected domains at high volume fraction with an apparent power law exponent of -0.35 ± 0.02. We also determined the correlation time of the fluctuations and inferred values for thermal diffusivity coefficient very near the critical point, above and below. The values were used to pinpoint the crossing of T_c within 13 μK.

DOI: 10.1103/PhysRevE.86.061501 PACS number(s): 64.75.−g, 78.15.+e, 02.30.Nw, 07.05.Pj

I. INTRODUCTION

There is a lack of data regarding phase separation in pure fluids in microgravity. Experiments investigating the critical behavior of pure fluids [1,2] and binary mixtures [3,4] have been performed with binary liquids near their miscibility critical point. In density-matched mixtures, gravity effects cannot be compensated for a long time [5]. The study of the long time evolution of fluctuations and phase separation in pure fluids needs gravity-free experiments [6–13]. The thermodynamic properties of critical fluids are indeed strongly affected by gravity because, among other properties, the compressibility of the fluid is very large near the critical point and the fluid compresses under its own weight [14,15]. Experiments in microgravity eliminate the complication due to fluid compressibility near the critical point.

Local density fluctuations activated by local thermal fluctuations induce small changes of the refractive index, which, in turn, induce fluctuations of light intensity passing through the fluid under investigation [16,17]. Density fluctuations in fluids near critical point are long ranged, a fact encompassed by the universal character of the power laws for many physical quantities [1,18–20].

In this paper, we applied an image processing technique, i.e., the dynamic structure factor (DSF) algorithm [21–24], and determined the structure factor (SF) and the correlation time of density fluctuations based on direct imaging experiments performed at 300 μK around the critical temperature ($T_c = 318.733$ K) of SF_6 in microgravity. The structure factor is the mean-squared amplitude of density fluctuations. We analyzed image sequences recorded very near the critical point. One advantage of this DSF technique is that the fluctuation image is defined as the difference between two normalized images a certain time interval Δt apart. By covering a wide range of delay time intervals Δt we were able to extract not only the SF, but also the optical background and the correlation time of density fluctuations. The data for large wave number q are consistent with a power law behavior SF $\propto q^{-2}$, which is a signature of the scale invariance of fluctuations very near the critical point. This result shows that very close to the critical point the SF of fluctuations is of Lorentzian type (q^{-2} scaling), since the liquid and vapor domains are just forming. During the late stages of phase separation, when the liquid-vapor interface is well developed, the SF evolves according to Porod's law (q^{-4} scaling) [19,25]. We also estimated the thermal diffusivity coefficient D_T from the correlation time [26]. The thermal diffusivity coefficient was previously estimated by Guenoun *et al.* [7] by using turbidity measurements with less accuracy than the present work.

 ©2012 American Physical Society

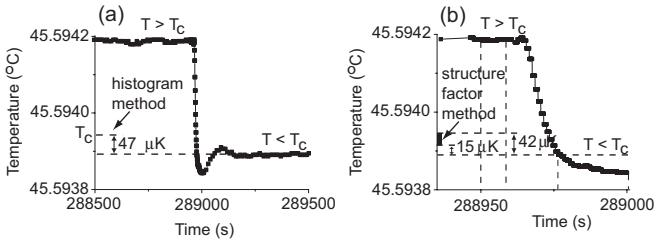

FIG. 1. Temperature measured by a thermistor placed inside the walls of the SCU vs the time stamp marked by Alice 2 instrumentation on recorded images over 1000 s around T_c (a) and a focused view only on the time interval very near above and below T_c (b). Phase separation occurs during this 300 μK thermal quench (a). Based on the histogram method, the estimated position of critical temperature is 47 μK above the lower plateau (a) [34]. Our current estimation based on the thermal diffusivity coefficient is between 15 and 42 μK above the lower plateau (b). For convenience, the origin of time was shifted to 288 950.00 s. The first pair of vertical dashed lines (b) marks the duration of recording analyzed for $T > T_c$, i.e., 0.00 s $< t <$ 8.00 s, which corresponds to image frames from zero to 200. The second pair of vertical dashed lines (b) marks the duration of recording analyzed for $T < T_c$, i.e., 28.12 s $< t <$ 51.12 s, which corresponds to image frames from 703 to 1278.

II. EXPERIMENTAL SETUP

A. General

The Alice 2 facility [5,27] used direct imaging of density fluctuations near the critical point of the pure fluid SF_6 in microgravity conditions. The fluid inside the sample cell unit (SCU) was prepared at the critical density, i.e., $\langle\rho^*\rangle = (\langle\rho\rangle - \rho_c)/\rho_c = \pm 0.02\%$, where $\langle\rho\rangle$ is the mean density and ρ_c is the critical density [28]. The fluid was held at a constant initial temperature above critical temperature ($T > T_c$) for about 40 min. Subsequently, a 300 μK thermal quench quickly decreased the SCU temperature below T_c and held it constant for approximately 40 min [Fig. 1(a)]. The experimental observation of critical opalescence phenomena, which is outside the scope of this paper, was used to approximately pinpoint the moment the system crosses T_c. In addition, because the fluid separated during this 300 μK thermal quench, we concluded that T_c was located between the initial and the final temperature plateaus shown in Fig. 1(a) [29].

The Alice 2 instrumentation writes on recorded images a time stamp, measured from the beginning of the experiment. This paper only investigates the formation of liquid and vapor domains during the very early stage of the phase separation phenomenon that occurs very close to T_c. Above critical temperature ($T > T_c$), we only analyzed images starting at $t =$ 288 950.00 s, which was labeled as image frame zero, up to $t =$ 288 958.00 s, i.e., image frame number 200 [Fig. 1(b)]. Below critical temperature ($T < T_c$) we analyzed images starting at $t =$ 288 978.12 s, i.e., image frame number 703, up to $t =$ 289 001.12 s, i.e., image frame number 1278 [Fig. 1(b)]. For convenience, 288 950.00 s were subtracted from all time stamps.

The temperature is measured by a thermistor inside the copper SCU wall, and its reading represents only approximately the actual temperature of the supercritical fluid. Among other factors, this approximate temperature reading is due to the fact that when the thermal quench command is issued, the cooling flux is more efficient on the SCU walls than in the bulk of the fluid, therefore, inducing a short (a few seconds) lag. It is also known that, in the supercritical region, the fluid inside the SCU suffers a fast adiabatic thermalization and reaches equilibrium on a much shorter time scale compared to the solid enclosure [30,31]. In addition, in spite of its low power value (<100 μW), a weak part of the laser beam power is absorbed in the sapphire windows, inducing a local weak temperature gradient in the fluid that can affect the estimation of the moment the fluid crosses T_c [32]. As a result, the actual times are shifted by about 5.5 s with respect to marked time. For the above reasons, we assumed that the actual temperature of the fluid on the lower plateau is 300 μK below the temperature of the well-stabilized upper plateau [33], despite the spurious short-term wiggling of the temperature reported by the thermistor inside the SCU wall [Fig. 1(a)]. A more detailed description of the experiment is presented elsewhere [28,29,34].

B. Optics

The density fluctuations were visualized through light transmission normal to the sapphire windows of the SCU using a He-Ne laser with 632.8 nm wavelength and about 100 μW maximum power. The laser stability after 1 h was estimated to be better than 0.3%. An optical microscope of 3 μm resolution was used to record a small region (less than 1 mm^2) of the SCU with a sampling rate of 25 Hz [35]. Here we analyze about 200 images (8 s of recording) above T_c, respectively, about 575 images (23 s of recording) below T_c. We cropped the largest possible square area of 190 $\times$ 190 pixels out of the original 256 $\times$ 256 pixel image of the SCU, which corresponds to a

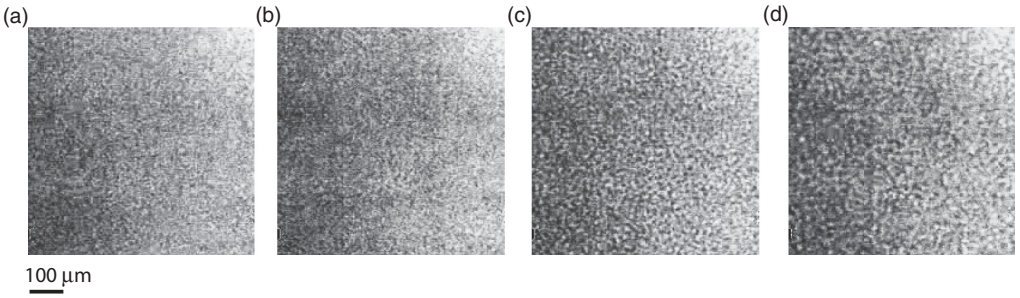

FIG. 2. Typical cropped image above T_c [(a) and (b)] and below T_c [(c) and (d)]. Images recorded 5 s before (a) and right at the end (b) of the 40-min-long upper plateau ($T > T_c$). Images recorded 10 s (c) and 20 s (d) into the lower temperature plateau ($T < T_c$).

0.9 mm × 0.9 mm visual field, in order to eliminate some recording markers written by Alice 2 instruments directly on images (time elapsed since the beginning of the experiment, etc.) The entire recording analyzed in this paper covers only phenomena happening during the *very early stages of the phase separation* [see Fig. 1(b)].

The small-scale bright and dark regions in Fig. 2 correspond to domains of larger and, respectively, smaller values for refractive index, or density. The large-scale intensity variation is due to changes in image illumination. Above T_c [Figs. 2(a) and 2(b)], only fluctuations are visible in recorded images. Below T_c [Figs. 2(c) and 2(d)], growing phase separated interconnected domains are clearly visible even during the early stages after crossing the critical temperature.

III. IMAGE PROCESSING TECHNIQUE

The image processing algorithm is as follows.

(1) Image normalization: In order to reduce the effect of variable light intensity, each cropped image (see Fig. 2) was normalized:

$$i(\boldsymbol{x},t) = I(\boldsymbol{x},t)/\langle I(\boldsymbol{x},t)\rangle,$$

where $I(\boldsymbol{x},t)$ is the intensity of the two-dimensional image and $\langle I(\boldsymbol{x},t)\rangle$ is the spatial average over all pixel positions in the image $I(\boldsymbol{x},t)$.

(2) Fluctuation image: It is the difference between two normalized images separated by a time delay Δt,

$$\delta i(\boldsymbol{x},t,\Delta t) = i(\boldsymbol{x},t+\Delta t) - i(\boldsymbol{x},t).$$

(3) Time-dependent structure function: This requires first the computation of the two-dimensional fast Fourier transforms (FFT2) for each fluctuation image

$$\delta i(\boldsymbol{q},t,\Delta t) = \mathrm{FFT2}(\delta i(\boldsymbol{x},t,\Delta t)),$$

from which the corresponding power spectrum is computed. The time-dependent structure function $c_m(\boldsymbol{q},\Delta t)$ is the ensemble, or temporal, average of all power spectra in a set of images with a fix time delay Δt [21–23]:

$$c_m(\boldsymbol{q},\Delta t) = \overline{|\delta i(\boldsymbol{q},t,\Delta t)|_t^2}.$$

We performed ensemble (temporal) averages of power spectra over sets of 64 successive images.

(4) Radial average of the time-dependent structure function: Due to the radial symmetry of the power spectrum, $c_m(\boldsymbol{q},\Delta t)$ was averaged over small ranges of wave vector $|\boldsymbol{q}|$ [23], where $q = |\boldsymbol{q}|$:

$$C_m(q,\Delta t) = \overline{c_m(\boldsymbol{q},\Delta t)_{|q|}}.$$

The dynamic structure factor algorithm for image processing is based on the definition of the fluctuating image $\delta i(\boldsymbol{x},t,\Delta t)$, whose spatial power spectrum average gives the time-dependent structure function $c_m(\boldsymbol{q},\Delta t)$. This approach has been previously used to remove the effect of slow drifts in the recorded signal [36]. This method is appropriate in our case since we investigate the density fluctuations due to a significant jump in temperature (300 μK) very near the critical point [Fig. 1(b)]. The time-dependent structure function $c_m(\boldsymbol{q},\Delta t)$ is the result of calculating the structure factor of a difference signal rather than of the signal itself. The radial average of the time-dependent structure function $c_m(\boldsymbol{q},\Delta t)$, which was calculated over rings of unit width in the discrete Fourier space, is related to the structure factor $S(q)$ and the normalized correlation function $g(q,\Delta t)$ as follows [21,22]:

$$C_m(q,\Delta t) = 2[[S(q)T(q)][1-g(q,\Delta t)] + B(q)], \quad (1)$$

where $T(q)$ is the transfer, or sensitivity, function of the optical method employed and $B(q)$ is a background term. The normalized correlation function is

$$g(q,\Delta t) = \exp[-\Delta t/\tau(q)], \quad (2)$$

where $\tau(q)$ is the lifetime of density fluctuations. For a small time delay, $\Delta t \to 0$, the normalized correlation function $g(q,\Delta t)$ should became unity and decrease to zero for large time delays. By fitting the radial average of the time-dependent structure function $C_m(q,\Delta t)$ to Eqs. (1) and (2), we determined the product $S(q)T(q)$, $\tau(q)$, and $B(q)$. In general, the power spectrum of the resultant images includes both the SF, $S(q)$, which measures the spatial distribution of the fluctuations, and the characteristic transfer function $T(q)$ of the optical method employed. Unfortunately, the two signals, $S(q)$ and $T(q)$, cannot be separated using image processing. However, the slope of the structure factor $S(q)$ at large values of the wave vector is seemingly the same as the slope of the product $S(q)T(q)$ (see the Appendix).

Since we used $N = 190$ pixels and the CCD resolution was $\Delta x \approx 3$ μm, the minimum wave vector is of the order of $q_{\min} = 1/(190 \times 3.1\ \mu\mathrm{m}) \approx 17\ \mathrm{cm}^{-1}$. Throughout this paper, all power spectra are given with the reduced wave vector $q^* = q/q_{\min}$ in arbitrary units (arb. units). The $q_{\min} = 17\ \mathrm{cm}^{-1}$ factor can be used to find the wave vector $q = q^* q_{\min}$ in cm^{-1} units. Since there were only $N = 190$ pixels in the cropped image ($1 < q^* < 190$), it results that the wave vector q in our experiment covered the range 17–2285 cm^{-1}. Furthermore, the power spectra for very small wave vectors ($q^* \ll 100$ arb. units) are affected by significant errors because the small radius $|q|$ determines a poor ensemble statistical average. For large wave vectors, the number of pixels (independent samples) in a single ring of the radial average of the power spectrum increases as $n\pi$, in which n is the number of the channel varying from 1 to $N/\sqrt{2}$. For example, at the maximum wave vector for our experiments, n is about $190/\sqrt{2} \approx 135$, resulting in over 400 statistically independent samples for a single wave vector, which is a reasonably good statistics.

IV. RESULTS

We computed the radial average of the time-dependent structure function $C_m(q,\Delta t)$ for different delay times Δt which were multiples of the 1/25 s sampling rate. The saturation of structure function $C_m(q,\Delta t)$ is determined by a significant decrease of correlation between images that are too far apart. The structure functions $C_m(q,\Delta t)$ were fitted with Eqs. (1) and (2) in order to extract the SF, the background noise, and the correlation time of fluctuations.

Very close to the critical point, the SF, which is the mean-squared amplitude of density fluctuations, is analytically captured by a Lorentzian

$$S(q) = S_0/[1+(q/q_c)^2], \quad (3)$$

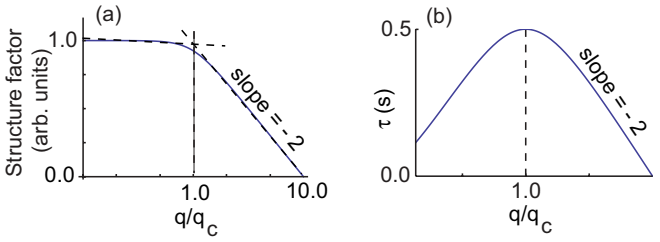

FIG. 3. (Color online) Log-log plot of the theoretical Lorentzian (a), and the log-log plot of the theoretical correlation time (b). For small wave vectors ($q/q_c \ll 1$), the SF has a very small slope. For large wave vectors ($q/q_c > 1$), the power law with an exponent of -2 indicates a Lorentzian behavior.

where S_0 is a constant and q_c is the critical value of the wave number. Figure 3(a) shows a log-log plot of the theoretical SF with $S_0 = 1$ arbitrary units. The correlation time represents the lifetime of the fluctuation [21]. For wave vectors $q > q_c$, the correlation time is well approximated by $1/(D_T q^2)$, where D_T is the thermal diffusivity constant (see Sec. IV A).

A. Estimation of SF and the correlation time of fluctuations above critical temperature

Dynamic structure factor algorithm allows SF to be estimated without prior measurements of the optical background by fitting the time-dependent structure function $C_m(q,\Delta t)$ [see Figs. 4(a) and 5(a)] with Eq. (1). Furthermore, the optical background is also obtained with this dynamic structure factor algorithm. We used the ratio of the SF against the background to determine the acceptable range of the wave vector for which the signal-to-noise ratio is high enough. We found that the amplitude of the background noise was at least one order of magnitude smaller than the SF, except for very low wave vectors ($q^* < 10$ arb. units).

Typical SF fitting results above critical temperature ($T > T_c$) are shown in Fig. 4(b). The image frames for $T > T_c$ are numbered from zero (at $t = 288\,950.00$ s) up to 200 [Fig. 4(b)]. The dynamic structure factor algorithm [see Eqs. (1) and (2)] also allowed us to compute the correlation time [see Fig. 4(c)] based on fluctuating images (Fig. 2).

The log-log plots of the SFs versus the wave vector q show two regions of interest [Fig. 4(b)]. For small wave vectors ($q^* < 100$ arb. units) we found that the SF is almost flat and presents a significant error due to very poor statistics over a very small number of wave numbers. For large wave numbers ($q^* > 100$ arb. units) we found that the SF has a larger negative slope of -2.19 ± 0.02 (image set 104–168, solid squares), respectively -2.33 ± 0.02 (image set 136–200, solid circles) [Fig. 4(b)]. As seen in Fig. 3(a), a truly Lorentzian structure factor should be almost q independent for $q \ll q_c$ and shows a power-law-like behavior for $q \gg q_c$ with an exponent that asymptotically approaches -2 [15,19,37].

Estimating the thermal diffusivity coefficient of homogeneous systems from the correlation time: The typical correlation time for fluctuations should obey the Kawasaki theory [26],

$$\tau^{-1} \propto D_T q^2, \tag{4}$$

if $q\xi_- \ll 1$ (hydrodynamic regime), where D_T is the thermal diffusivity coefficient. On the other hand, for $q\xi_- \gg 1$ (critical regime), the correlation time should scale as $\tau^{-1} \propto A q^{3.068}$, where A is a constant [38]. For the temperature quench of $\Delta T = T - T_c \approx 300\ \mu$K, the estimated average correlation length is $\xi_- \approx 1.95 \times 10^{-4}$ cm [34]. Since in our experiment $17\ \text{cm}^{-1} < q < 2285\ \text{cm}^{-1}$, the product $q\xi_-$ is in the range $3.3 \times 10^{-2} < q\xi_- < 0.4$, which is definitely not $q\xi_- \gg 1$ as it is required for the critical regime. As a result, our experimental data fall in the *hydrodynamic regime* where the correlation time should scale according to Eq. (4). We used a Levenberg-Marquardt least-squares fitting algorithm to estimate D_T. For the homogeneous system above critical temperature, we found that D_T is in the range $(2.1\text{–}2.6) \times 10^{-8}\ \text{cm}^2/\text{s}$.

Estimation of the critical temperature from thermal diffusivity coefficient: As proposed by Luettmer-Strathmann *et al.* [39], and validated by Wilkinson *et al.* [40] for SF_6, the thermal diffusivity D_T scaling law is

$$D_T = D_{0b}\Delta\tau^{\gamma} + D_{0c}\Delta\tau^{\nu+x_\eta}, \tag{5}$$

where $\Delta\tau = |(T - T_c)/T_c|$ is the reduced temperature. For $T > T_c$, the coefficients are $D_{0b}^{+} = 1.32 \times 10^{-2}\ \text{cm}^2/\text{s}$, $D_{0c}^{+} = (4.05 \pm 0.24) \times 10^{-4}\ \text{cm}^2/\text{s}$, $T_c = 318.733$ K, $\nu = 0.63$ is the critical exponent of the correlation length, $x_\eta = 0.04$ is the critical exponent of the shear viscosity, and $\gamma = 1.24$ [41]. We used the above estimations of D_T to infer the reduced temperature $\Delta\tau = |(T - T_c)/T_c|$ from Eq. (5). Our current estimations

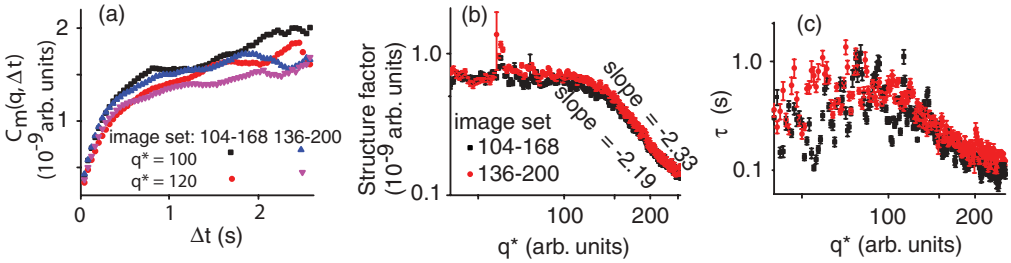

FIG. 4. (Color online) Time-dependent structure functions (a) saturate for large time delays Δt. Log-log plots of the experimental structure factors (b) and correlation times (c) above critical temperature. For small wave vectors ($q \ll q_c$), the SF has a very small slope. For large wave vectors ($q > q_c$), a power law emerges with an exponent (-2) close to the theoretically predicted Lorentzian. Ensemble averages were computed over sets of 64 images. Log-log plot of the experimental correlation time values vs the wave number q^* at different times shows two regions of interest. For small wave numbers ($q < q_c$) the data are too spread out to give a consistent trend. For large wave vectors, the correlation time of fluctuations scales with q^{-2}.

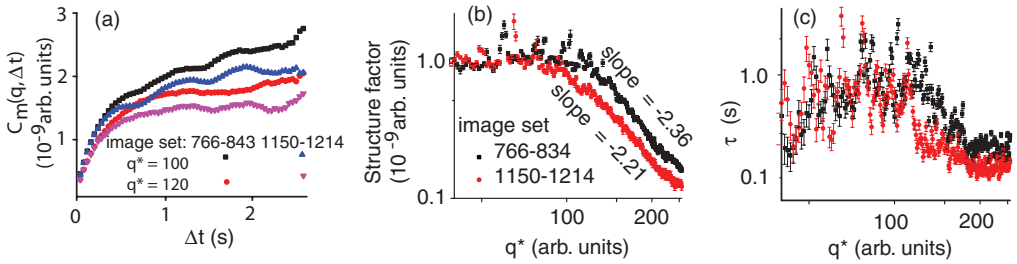

FIG. 5. (Color online) Time-dependent structure functions (a) saturate for large time delays Δt. Log-log plots of the experimental structure factors (b) and correlation times (c) below critical temperature. For small wave numbers ($q < q_c$) the data are too spread out to give a consistent trend. For large wave vectors ($q > q_c$), a power law emerges with an exponent slightly larger than -2 (a).

based on the dynamic structure factor algorithm place the critical point somewhere between 15 and 42 μK above the lower temperature plateau. This value is in agreement with our previous estimation obtained with a different method [34] for the same set of experiments. Based on the histogram method [34], T_c was found between 36 and 67 μK (with the average at 47 μK) above the lower temperature plateau.

B. Estimation of SF and the correlation time of fluctuations below critical temperature

Using the same dynamic structure factor algorithm as in the previous section, we fitted the time-dependent structure function $C_m(q,\Delta t)$ [see Fig. 5(a)] with Eqs. (1) and (2) in order to calculate the structure factor [Fig. 5(b)] and correlation time [Fig. 5(c)] for temperatures below T_c. Ensemble (temporal) averages were computed over sets of 64 power spectra and for $T < T_c$ we analyzed image frames from 703 (at $t =$ 288 978.12 s) up to 1278 (Fig. 5).

Below T_c and for small wave numbers ($q^* < 100$ arb. units) the DSF is flat, whereas for large wave numbers ($q^* > 100$ arb. units) the exponents are -2.36 ± 0.02 (image set 766–834, solid squares), respectively, -2.21 ± 0.02 (image set 1150–1214, solid circles) [Fig. 5(b)]. The slope of the structure factor [Fig. 5(b)] for $q \gg q_c$ is slightly larger than the Lorenzian characteristic exponent of -2 [15,19,37]. At the same time, the exponent is not large enough to match the value of -4, which is characteristic for domains with a well-developed liquid-vapor interface [19,25]. Therefore, we concluded that our data capture a region where liquid and vapor domains are just forming.

Below critical temperature ($T < T_c$), the structure factor and the correlation time allowed us to investigate the universality class of phase separation processes (Sec. IV C).

C. Universal power law exponents for the scaled wave vector versus time during the early stages of phase separation

Using SF data, we estimated the position of the critical, or crossover, wave vector q_c between the (almost) flat and the power law regions [Fig. 3(a)]. For $T < T_c$, the position of q_c shifts over time toward smaller wave vector values, showing that the characteristic length of the interconnected clusters increased due to phase separation. In order to uncover possible universal growth laws for the interconnected clusters during the very early stages of phase separation, we plotted in Fig. 6 the normalized crossover wave vector $k^* = q_c\xi_-$ versus the normalized time $t^* = t/t_\xi$ [34]. The correlation length is computed according to [18,19,42]

$$\xi = \xi_{0-}((T_c - T)/T_c)^{-\nu} \tag{6a}$$

and

$$t_\xi = 6\pi\eta\xi_-^3/k_BT_c = 1.714\,42 \times 10^{17}\xi_-^3, \tag{6b}$$

where $\xi_{0-} = 1.926/2 \times 10^{-10}$ m, $T_c = 318.733$ K, $\nu = -0.6304$, η is the shear viscosity [15,20,28,43], and k_B is Boltzmann's constant. Based on a different image processing technique (histogram method), we previously estimated for the same set of images that T_c is about 47 μK above the lower temperature plateau shown in Fig. 1 [34]. Based on data in Fig. 1, the absolute time, measured from the beginning of the recordings from which we subtracted the reference time 288 950 s [see Fig. 1(b)] when the system crossed T_c was $t_0 = 23.5$ s. For each set of 64 images below T_c we determined a SF and estimated q_c (Fig. 6). The time stamp assigned to each set of 64 images below T_c is the difference between the absolute time marked on the first image of the set and t_0.

The temperature difference $T_c - T$ necessary for ξ_- computation was defined the same way as the elapsed time. Depending on the growing domain volume fraction with respect to a "critical" value of ≈30%, two phase separation mechanisms are dominant [44–46]: (i) Bubble growth by coalescence induced by Brownian collisions. In the scaled graph of Fig. 6 (dashed line) it shows at all times a power law

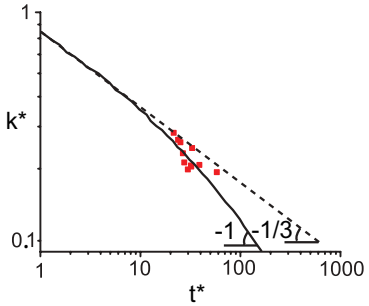

FIG. 6. (Color online) Log-log plot of the normalized crossover wave vector $k^* = q_c\xi$ vs the normalized elapsed time $t^* = t/t_\xi$ below critical temperature. Depending on the phase separation mechanism, two universal curves are present: (i) bubble growth (dashed line) with a slope of $-1/3$ at all times, and (ii) interconnected domain growth (solid line) with a slope of -1 at all times (adapted after Ref. [13]).

with a slope of $-1/3$. (ii) Interconnected domain growth (solid line) with a slope of -1 at all times. Our data are concerned with the interconnected domain growth (see Fig. 2) and indeed obey the evolution (ii) (Fig. 6). When fitted to a power law, the data show an apparent power law exponent -0.35 ± 0.02. The scaling law was obtained assuming that T_c was 47 μK above the lower plateau in Fig. 1(a) and the time when the system crossed T_c was $t_0 = 288\,973.5$ s (after Refs. [34,47]).

V. CONCLUSIONS

We used direct observation images recorded in microgravity for SF_6 very close to T_c in order to determine the SF of density fluctuations and the correlation time $\tau(q)$. The SFs fit well to the theoretical Lorentzian type structure factor Eq. (3) and give us the crossover wave number q_c which determines the correlation length ξ_- of fluctuations. The q^{-2} scaling of the SF during the very early stages of phase separation shows that the liquid and vapor domains just formed. When scaled with ξ_-, [Eq. (6a)] and time normalized by the critical fluctuation lifetime t_ξ [Eq. (6b)], the scaled wave vector $k^* = q_c\xi_-$ obeys the universal scaled growth for interconnected, high volume fraction, liquid-vapor domains.

The thermal diffusivity coefficient D_T was determined from the correlation time of density fluctuations so close to the critical point (a few tens of μK). Furthermore, using theoretical scaling laws for SF_6 near T_c [39,40], we found estimations of the critical point position that are consistent with previous results obtained using the histogram method [34]. It is interesting to note that the employ of direct imaging techniques [17], as used in this study, which take advantage of local measurements, gives accuracies comparable to the classical scattering techniques where fluctuations are averaged over the illuminating beam.

ACKNOWLEDGMENTS

This work was supported by SCSGC-NASA grant to A.O. and S.A.O., and R&D grants to A.O. from the College of Charleston. S.A.O. acknowledges NSF CAREER IOS-1054914 for support. Microgravity experiments were carried out with the support of NASA Grants No. NAG3-1906 and No. NAG3-2447 to J.J.H. D.B. acknowledges CNES support.

APPENDIX

The transfer or sensitivity function, $T(q)$ is determined by the transmission function of the mask placed in the focal plane of the optical setup. For example, in the case of the shadowgraph technique, no spatial filtering is used on the light beam and the corresponding transfer function is $T(q) = 4\sin^2[q^2z/(2k)]$, where k is the wave number for incident light, z is the distance between the sample and the plane imaged onto the sensor, and θ is the scattering angle. In the case of the schlieren technique, the intensity mask in the Fourier plane is typically a sharp blade covering half of the focal plane [17,21]. The blade blocks half of the main beam and one of the two symmetrically scattered beams at opposite angles. The interference at the visualization plane is determined only by the interference of half the transmitted beam and one out of the two symmetrically scattered beams. Therefore, the transfer function of the schlieren method is $T(q) = 1$.

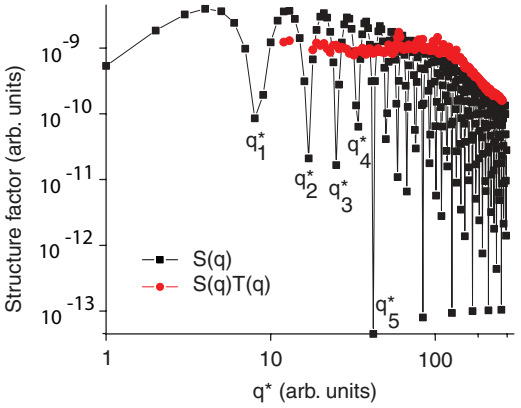

FIG. 7. (Color online) Experimentally determined product $S(q)T(q)$ based on the dynamic structure factor algorithm (solid circles). Assuming that the transfer function of the direct imaging method is $T(q) = 4\sin^2[q^2z/(2k)]$, the structure factor $S(q)$ was determined (solid squares). The zeros q_n^* of the transfer function $T(q)$ are closer and closer such that for $q^* > 10$ arbitrary units the distance between successive zeros is below the experimental resolution. For large wave vectors, $q^* > 100$ arbitrary units, the slope of $S(q)$ is seemingly identical to the slope of $S(q)T(q)$.

In the case of no spatial filtering on the beam (direct imaging or shadowgraph) the dynamic structure factor algorithm (1) computes only the product of the structure factor $S(q)$ and $T(q) = 4\sin^2[q^2z/(2k)]$. The actual structure factor $S(q)$ can be readily computed for known $T(q)$. However, significant uncertainty occurs during $S(q)$ estimation when $T(q) = 0$, i.e., for $q^2z/(2k) = n\pi$, with $n = 1,2,3,\ldots$. The corresponding values of the wave number at which $T(q)$ vanishes and, therefore, leads to high uncertainty on the structure factor estimations are $q_n \approx 2\pi\sqrt{n/(z\lambda)}$. For our experimental setup, $\lambda = 628.3$ nm and $z \approx 1$ m, which leads to $q_n \approx 79.27\sqrt{n}$ cm^{-1}. Given that $q_c = 17$ cm^{-1}, it means that the dimensionless wave number is $q_n^* \approx 4.66\sqrt{n}$ arbitrary units. While the integer index n increases, the wave numbers q_n^* at which $T(q)$ vanishes are closer and closer. The distance between two successive zeros of $T(q)$ is $\Delta q_{n+1,n}^* \approx 4.66(\sqrt{n+1} - \sqrt{n})$, which falls below the resolution threshold of our method when $\Delta q_{n+l,n}^* < 1$ arbitrary units, i.e., for all values of $n > 5$. As a result, for all wave vectors above $q^* \approx 4.66\sqrt{5} \approx 10$ arbitrary units the distance between two successive zeros of $T(q)$ is smaller than the experimental resolution. Therefore, for $q^* > 10$ arbitrary units, $T(q)$ oscillates so fast that only its average contributes to the product $S(q)T(q)$. Furthermore, since we only need to estimate the slope of the structure factor for large wave numbers, i.e., $q^* > 100$ arbitrary units, it is safe to approximate $T(q)$ by its average value, i.e., $\frac{1}{2\pi}\sqrt{\frac{z\lambda}{n}}\int_0^{2\pi\sqrt{n/z\lambda}}[\sin(\frac{z\lambda q^2}{4\pi})]^2 dq$. The above integral converges very fast for large values of n to its $n \to \infty$ limit, which is $\frac{1}{2}$. As a result, the transfer function $T(q)$ does not alter the slope of the dynamic structure factor $S(q)$ for all measurements above $q^* > 100$ arbitrary units (see Fig. 7). This is the reason we estimated the slope of the structure factor for large values of the wave vector directly from the product $S(q)T(q)$.

[1] D. S. Cannell, Phys. Rev. A **12**, 225 (1975).
[2] D. Beysens, in *Materials Sciences in Space, A Contribution to the Scientific Basis of Space Processing*, edited by B. Feuerbacher, H. Hamacher, and R. J. Naumann (Springer, Berlin, 1986), p. 191.
[3] E. D. Siggia, Phys. Rev. A **20**, 595 (1979).
[4] P. Guenoun, F. Perrot, and D. Beysens, Phys. Rev. Lett. **63**, 1152 (1989).
[5] D. Beysens, P. Guenoun, and F. Perrot, J. Phys.: Condens. Matter **2**, SA127 (1990).
[6] Y. Garrabos, B. Le Neindre, P. Guenoun, B. Khalil, and D. Beysens, Europhys. Lett. **19**, 491 (1992).
[7] P. Guenoun, B. Khalil, D. Beysens, Y. Garrabos, F. Kammoun, B. Le Neindre, and B. Zappoli, Phys. Rev. E **47**, 1531 (1993).
[8] P. Guenoun, D. Beysens, F. Perrot, Y. Garrabos, and A. Kumar, J. Phys.: Condens. Matter **6**, A199 (1994).
[9] M. Barmatz, I. Hahn, J. A. Lipa, and R. V. Duncan, Rev. Mod. Phys. **79**, 1 (2007).
[10] C. Bartscher and J. Straub, Int. J. Thermophys. **23**, 77 (2002).
[11] B. Zappoli, R. Kuhl, J. Robey, and A. Ivanov, Acta Astronaut. **53**, 963 (2003).
[12] F. Perrot, D. Beysens, Y. Garrabos, T. Fröhlich, P. Guenoun, M. Bonetti, and P. Bravais, Phys. Rev. E **59**, 3079 (1999).
[13] D. Beysens and Y. Garrabos, Physica A **281**, 361 (2000).
[14] V. Emelianov, A. Lednev, V. Polezhaev, A. Ivanov, G. Putin, A. Zyuzgin, D. Beysens, and Y. Garrabos, Microgravity Sci. Technol. **16**, 164 (2005).
[15] M. R. Moldover, J. V. Sengers, R. W. Gammon, and R. J. Hocken, Rev. Mod. Phys. **51**, 79 (1979).
[16] P. Carles, J. Supercrit. Fluids **53**, 2 (2010).
[17] S. P. Trainoff and D. S. Cannell, Phys. Fluids **14**, 1340 (2002).
[18] C. Domb, J. L. Lebowitz, and J. Lebowitz, *Phase Transitions and Critical Phenomena* (Academic, London, 2001).
[19] A. Onuki, *Phase Transition Dynamics* (Cambridge University Press, Cambridge, UK, 2002).
[20] H. Furukawa, Adv. Phys. **34**, 703 (1985).
[21] F. Croccolo, Ph.D. dissertation, Università degli Studi di Milano, 2006.
[22] F. Croccolo, D. Brogioli, A. Vailati, M. Giglio, and D. S. Cannell, Appl. Opt. **45**, 2166 (2006).
[23] F. Croccolo, D. Brogioli, A. Vailati, M. Giglio, and D. S. Cannell, Phys. Rev. E **76**, 041112 (2007).
[24] A. Vailati, R. Cerbino, S. Mazzoni, C. J. Takacs, D. S. Cannell, and M. Giglio, Nat. Commun. **2**, 290 (2011).
[25] G. Porod, Kolloid Zeit. **124**, 83 (1951); **125**, 51, (1951).
[26] K. Kawasaki, Ann. Phys. **61**, 1 (1970).
[27] D. Beysens and Y. Garrabos, Acta Astronaut. **48**, 629 (2001).
[28] C. Lecoutre, Y. Garrabos, E. Georgin, F. Palencia, and D. Beysens, Int. J. Thermophys. **30**, 810 (2009).
[29] A. Oprisan, Ph.D. dissertation, University of New Orleans, 2006.
[30] A. Onuki, H. Hao, and R. A. Ferrell, Phys. Rev. A **41**, 2256 (1990).
[31] J. Straub, L. Eicher, and A. Haupt, Phys. Rev. E **51**, 5556 (1995).
[32] D. Beysens, Y. Garrabos, V. S. Nikolayev, C. Lecoutre-Chabot, J.-P. Delville, and J. Hegseth, Europhys. Lett. **59**, 245 (2002).
[33] M. Bonetti, F. Perrot, D. Beysens, and Y. Garrabos, Phys. Rev. E **49**, R4779 (1994).
[34] A. Oprisan, S. A. Oprisan, J. J. Hegseth, Y. Garrabos, C. Lecoutre-Chabot, and D. Beysens, Phys. Rev. E **77**, 051118 (2008).
[35] J. Hegseth, A. Oprisan, Y. Garrabos, V. S. Nikolayev, C. Lecoutre-Chabot, and D. Beysens, Phys. Rev. E **72**, 031602 (2005).
[36] E. O. Schultz-DuBois and I. Rehberg, Appl. Phys. **24**, 323 (1981).
[37] P. Guenoun, R. Gastaud, F. Perrot, and D. Beysens, Phys. Rev. A **36**, 4876 (1987).
[38] H. C. Burstyn, J. V. Sengers, J. K. Bhattacharjee, and R. A. Ferrell, Phys. Rev. A **28**, 1567 (1983).
[39] J. Luettmer-Strathmann, J. V. Sengers, and G. A. Olchowy, J. Chem. Phys. **103**, 7482 (1995).
[40] R. A. Wilkinson, G. A. Zimmerli, H. Hao, M. R. Moldover, R. F. Berg, W. L. Johnson, R. A. Ferrell, and R. W. Gammon, Phys. Rev. E **57**, 436 (1998).
[41] R. Guida and J. Zinn-Justin, J. Phys. A (Math. Gen.) **31**, 8103 (1998).
[42] D. Chandler and I. Oppenheim, J. Chem. Phys. **49**, 2121 (1968).
[43] J. J. Hurly, D. R. Defibaugh, and M. R. Moldover, Int. J. Thermophys. **21**, 739 (2000).
[44] V. S. Nikolayev, D. Beysens, and P. Guenoun, Phys. Rev. Lett. **76**, 3144 (1996).
[45] C. Sagui and M. Grant, Phys. Rev. E **59**, 4175 (1999).
[46] C. Sagui, D. S. O'Gorman, and M. Grant, Scanning Microsc. **12**, 3 (1998).
[47] A. Oprisan, J. J. Hegseth, G. R. Smith, C. Lecoutre, Y. Garrabos, and D. A. Beysens, Phys. Rev. E **84**, 021202 (2011).